Monthly Notices
of the
ROYAL ASTRONOMICAL SOCIETY

MNRAS **478,** 4575–4589 (2018) doi:10.1093/mnras/sty1303

Optical observations of the 2002cx-like supernova 2014ek and characterizations of SNe Iax

Linyi Li,[1⋆] Xiaofeng Wang,[1⋆] Jujia Zhang,[2,3,4] Iair Arcavi,[5,6†] Tianmeng Zhang,[7,8] Liming Rui,[1] Griffin Hosseinzadeh,[5,6] D. Andrew Howell,[5,6] Curtis McCully,[5,6] Kaicheng Zhang,[1] Stefano Valenti,[9] Jun Mo,[1] Wenxiong Li,[1] Fang Huang,[1,10] Danfeng Xiang,[1] Lifan Wang[11,12] and Xu Zhou[8]

[1] *Physics Department and Tsinghua Center for Astrophysics (THCA), Tsinghua University, Beijing 100084, China*
[2] *Yunnan Observatories (YNAO), Chinese Academy of Science s, Kunming 650216, China*
[3] *Key Laboratory for the Structure and Evolution of Celestial Objects, Chinese Academy of Sciences, Kunming 650216, China*
[4] *Center for Astronomical Mega-Science, Chinese Academy of Sciences, 20A Datun Road, Chaoyang District, Beijing 100012, China*
[5] *Las Cumbres Observatory, 6740 Cortona Dr Suite 102, Goleta, CA 93117-5575, USA*
[6] *Department of Physics, University of California, Santa Barbara, CA 93106-9530, USA*
[7] *Key Laboratory of Optical Astronomy, National Astronomical Observatories of China, Chinese Academy of Sciences, Beijing 100012, China*
[8] *School of Astronomy and Space Science, University of Chinese Academy of Sciences, Beijing 101408, China*
[9] *Department of Physics, University of California, Davis, CA 95616, USA*
[10] *Department of Astronomy, Shanghai Jiao Tong University, Shanghai 200240, China*
[11] *George P. and Cynthia Woods Mitchell Institute for Fundamental Physics & Astronomy, Texas A. & M. University, College Station, TX 77843, USA*
[12] *Purple Mountain Observatory, Chinese Academy of Sciences, Nanjing 210034, China*

Accepted 2018 May 9. Received 2018 May 9; in original form 2018 January 31

ABSTRACT

We present optical observations of supernova (SN) 2014ek, discovered during the Tsinghua University–National Astronomical Observatories, Chinese Academy of Sciences (NAOC) Transient Survey (TNTS), which shows properties that are consistent with those of SN 2002cx-like events (dubbed as SNe Iax). The photometry indicates that it is underluminous compared with normal SNe Ia, with the absolute V-band peak magnitude being -17.66 ± 0.20 mag. The spectra are characterized by highly ionized Fe III and intermediate-mass elements (IMEs). The expansion velocity of the ejecta is found to be $\sim$5000 km s^{-1} near the maximum light, only half of that measured for normal SNe Ia. The overall spectral evolution is quite similar to that of SN 2002cx and SN 2005hk, while the absorption features of the main IMEs seem to be relatively weaker. The ^{56}Ni mass synthesized in the explosion is estimated to be about 0.08 $M_\odot$ from the pseudo-bolometric light curve. Based on a large sample of SNe Iax, we examined the relations between peak luminosity, ejecta velocity, decline rate and peak $V - R$ colour, but did not find noticeable correlations between these observables, in particular when a few extreme events like SN 2008ha are excluded from the analysis. For this sample, we also studied the birthplace environments and confirm that they still hold the trend of occurring preferentially in late-type spiral galaxies. Moreover, SNe Iax tend to occur in large star-forming regions of their host galaxies, more similar to SNe Ibc than SNe II, favouring the idea that their progenitors should be associated with very young stellar populations. Nevertheless, the progenitors of SNe Iax may have relatively lower metallicity, as suggested by the evidence that they prefer to explode in outer regions of host galaxies.

Key words: supernovae: general – supernovae: individual: SN 2014ek.

1 INTRODUCTION

Supernovae (SNe) represent the final, explosive stage in the evolution of certain types of stars, playing important roles in diverse

⋆ E-mail: lily940809@163.com (LL) wang_xf@mail.tsinghua.edu.cn (XW)
† Einstein Fellow

aspects of astrophysics. With the dramatic increase in the number of SNe discovered over the past decade, numerous types and subtypes have been introduced to describe their diverse observational properties. In theory, SNe have been considered to form in two main channels: thermonuclear explosions of accreting white dwarfs (WDs) in binary systems and core-collapse (CC) explosions of massive stars. How different types of SNe are produced from different types of stars is not yet well understood. An accurate physical model of SNe is important not only for our understanding of late stages of stellar evolution but also for precision cosmology.

Among thermonuclear WD explosions, normal type Ia supernovae (SNe Ia) belong to the most common subclass and are well known as distance indicators to measure the expansion rate of the Universe (Riess et al. 1998; Perlmutter et al. 1999). They are generally believed to arise from explosions of accreting carbon–oxygen (CO) WDs with mass close to 1.4 $M_{\odot}$ in binary systems, although large scatter emerges in their observed properties. For example, some SNe Ia show weak features of intermediate-mass elements (IMEs) and prominent Fe II/Fe III lines, like the luminous subclass of SN 1991T (Filippenko et al. 1992), while others show strong features of IMEs and prominent Ti II lines, like the faint subclass of SN 1991bg (see reviews by Filippenko 1997). Aside from these subtypes, some exotic thermonuclear explosion events have also emerged in recent years as a result of the expansion of wide-field survey projects. One peculiar subclass has very high luminosity and strong absorption of unburned carbon in its spectra (Howell et al. 2006). Representative examples include SN 2007if (Scalzo, Aldering & Antilogus 2010) and SN 2009dc (Yamanaka et al. 2009), which could be due to explosions of super-Chandrasekhar-mass WDs (i.e. with mass $\gtrsim$2.0 $M_{\odot}$). The SN 2002cx-like SN represents another unusual subclass, which was initially noticed by Li et al. (2003) and is characterized by an SN 1991T-like pre-maximum spectrum (i.e. highly ionized Fe III), an SN 1991bg-like luminosity and low ejecta velocities.

There are currently about 45 SNe that have been identified as SN 2002cx-like subclass (also dubbed as SNe Iax) according to their spectral features. Compared with normal SNe Ia, SNe Iax are found to show obviously weaker absorption of IMEs in their spectra and relatively stronger spectral features of iron-group elements (IGEs) in the early phase. The expansion velocities measured from the spectra of SNe Iax are found to be only roughly half those of normal SNe Ia, ranging from ∼2000 to ∼8000 km s^{-1}. At late times, the spectra of normal SNe Ia are dominated by broad forbidden emission lines of IGEs, while SNe Iax show narrow permitted lines of IGEs (Jha et al. 2006). Photometrically, SNe Iax are found to be significantly fainter than normal SNe Ia, with an absolute peak magnitude ranging from about −13 mag to about −18 mag in the *V* band (Foley et al. 2013). Nevertheless, these low-luminosity SNe Iax do not show a faster decline rate (i.e. with a typical value of $\Delta m_{15}(B)\approx1.3$ mag), as expected from the Lira–Phillips relation found for normal SNe Ia (Phillips 1993). This indicates that SNe Iax have different energy sources, explosion mechanisms and/or progenitor systems compared with normal SNe Ia. Besides this, two SNe Iax (SN 2004cs and SN 2007J) are found to show the He I emission line in their spectra (Foley et al. 2013), suggesting that they might have more massive progenitor systems than SNe Ia. Nevertheless, the nature of the progenitor systems of SNe Iax is still highly debated.

Theoretically, the peculiar subclass of SNe Iax may arise from a less violent explosion of a C/O WD that has accreted He-rich material from a companion star and this could correspond to a pure deflagration when the SN fails to change from deflagration to detonation in the explosion (Phillips et al. 2007; Foley et al. 2009; Jordan et al. 2012; Kromer et al. 2013; and Liu et al. 2015). As an alternative, SNe Iax have also been proposed to result from core collapse explosion of massive stars, but with significant fallback on to a new-formed black hole (i.e. Valenti et al. 2009; Moriya et al. 2010), which is favoured by the fact that SNe Iax prefer to occur in late-time spiral galaxies and are associated with young stellar environments (Foley et al. 2009; Lyman et al. 2013). Analysis of the pre-explosion *Hubble Space Telescope* (*HST*) image, which may be the most effective way to constrain the progenitors of SNe, indicates that SN 2012Z may have a progenitor system consisting of a white dwarf and a companion that is a non-degenerate helium-star (McCully et al. 2014; Yamanaka et al. 2015). Note, however, that current members of the SNe Iax class show large differences in luminosity and spectral features, suggesting that this peculiar subclass may also come from a diverse set of progenitor systems or explosion models. Some members of the current sample of SNe Iax could be misclassified. A larger sample of SNe Iax is thus needed to address the observed diversities and their origins.

In this work, we present observations and study of another member of the 2002cx-like supernovae, SN 2014ek. Some statistical results based on a collection of current SNe Iax samples are also presented. This article is organized as follows. We describe our observations and data reduction in Section 2. Analysis of reddening, photometry and spectra of SN 2014ek is presented in Section 3. In Section 4, we discuss the luminosity, its correlation with photometric and spectroscopic parameters and the progenitor environments of SN 2014ek, along with other samples. Finally, we give a brief summary in Section 5.

2 OBSERVATION AND DATA REDUCTION

SN 2014ek was discovered on 2014 October 18.81 UT during the Tsinghua–National Astronomical Observatories, Chinese Academy of Sciences (NAOC) Transient Survey (TNTS: see Yao et al. 2015; Zhang et al. 2015). It exploded in the spiral galaxy UGC 12850, which seems to be a Sb galaxy from its SDSS images, with a relatively less prominent barred structure, as shown in Fig. 1. The coordinates of this SN are $\alpha = 23^{h}56^{m}06.55^{s}$, $\delta = +29^{\circ}22'42''.3$, approximately 7.0 arcsec east and 1.0 arcsec north from the centre of the host galaxy. The redshift of UGC 12850 is 0.023, consistent with that derived from the narrow Hα emission seen in the SN spectra, which corresponds to a distance modulus of 34.99±0.20 mag (Tully et al. 2013). A spectrum taken on 2014 October 22.76 UT with the 2.4-m telescope at LiJiang Gaomeigu Station of Yunnan Observatories matches the peculiar supernova SN 2002cx (Li et al. 2003) at about one week before maximum light. An expansion velocity of about 6000 km s^{-1} is inferred from the Si II 6355 absorption minima (Zhang & Wang 2014). As SN 2014ek was discovered at a relatively early phase, we triggered follow-up optical observations of this object, spanning the phase from about 6 days before to about 1 month after the *B*-band maximum light.

2.1 Optical photometry

The optical photometry of SN 2014ek was collected using the 0.8-m Tsinghua University–NAOC telescope (hereafter TNT) at Xinglong Observatory of NAOC, the Las Cumbres Observatory Global Telescope 1-m network (hereafter LCO) and the Lijiang 2.4-m telescope (LJT) of Yunnan Astronomical Observatories. The TNT and LJT observations were obtained in standard Johnson–Cousin *UBVRI* bands, while the LCO photometry was taken in the Johnson *BV* and

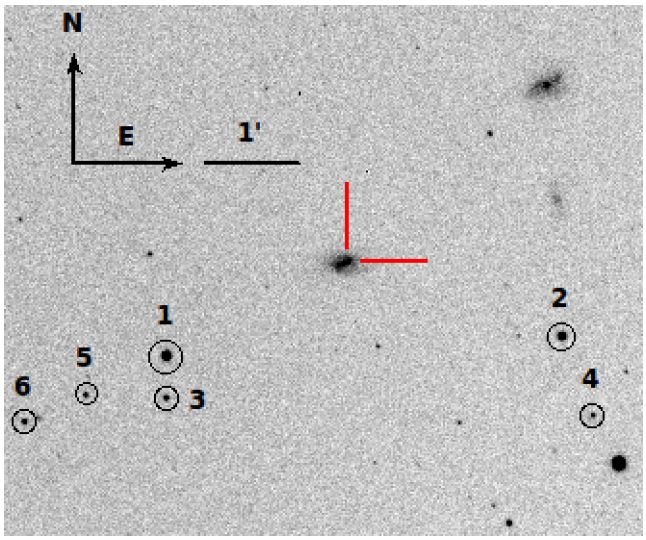

Figure 1. SN 2014ek in UGC 12850. This is an *R*-band image taken by the Lijiang 2.4-m telescope on 2014 October 31.63 UT. The supernova is located at the centre of the cross-hairs and six standard stars are marked. North is up and east is to the right.

Sloan *gri* filters. These observations covered the phases from 2014 October 22–2014 November 29.

All CCD images were pre-processed using standard IRAF[1] routines, including corrections for bias, flat field and removal of cosmic rays. As SN 2014ek is located close to the centre of UGC 12850, measurements of the SN flux will be affected by the galaxy light. Thus a template subtraction technique is applied to the observed images of SN 2014ek before performing photometry. The galaxy templates for the LCO, LJT and TNT data were taken on 2016 June 07.40, 2015 September 12.63 and 2015 November 13.15, respectively, which corresponds to 588.01, 319.24 and 381.27 days after *B*-band maximum light. The instrumental magnitudes of both the SN and reference stars were then measured from the subtracted images using aperture photometry.

To convert the instrumental magnitudes to the standard system, six reference stars marked in Fig. 1 were used to determine the photometric zero-points. The colour terms of the LCO, TNT and LJT and the extinction coefficients at the corresponding sites are taken from Valenti et al. (2016), Huang et al. (2012) and Zhang et al. (2014), respectively. The *UBVRI* and *ugri*-band magnitudes of the field stars are listed in Table 1. The Johnson *UBVRI* magnitudes of these comparison stars are transformed from the *ugri* magnitudes from the Sloan Digital Sky Survey (SDSS) Data release 9 catalogue (Ahn et al. 2012). The LCO *gri*-band magnitudes are also converted to the *BVRI*-band values to increase the data sampling in these wavebands. The transformation of the *UBVRI* magnitudes from SDSS *ugri* magnitudes is based on the empirical formula given in Jordi, Grebel & Ammon (2006). The final calibrated magnitudes of SN 2014ek are presented in Table 2. We did not apply additional magnitude corrections to the photometry from different telescopes (i.e. *S*-corrections; Stritzinger et al. 2002), as the *BVRI*-band magnitudes obtained from the three photometric systems are consistent with each other overall (i.e. within ∼0.05 mag) and accurate *S*-corrections between different systems need detailed information about the transmission curves of different filters, which is not available for the TNT system.

[1] IRAF is distributed by the National Optical Astronomy Observatories, which are operated by the Association of Universities for Research in Astronomy, Inc., under cooperative agreement with the National Science Foundation (NSF).

2.2 Optical spectroscopy

A total of nine low-resolution optical spectra were obtained for SN 2014ek, covering the phases from $t \sim -5.1$ days to +25.3 days relative to the *B*-band maximum light. Seven of these spectra were obtained with the YFOSC system mounted on the Lijiang 2.4-m telescope and fluxes of these spectra were corrected with photometric results from the LJT. Another two spectra were obtained with FLOYDS mounted on the 2.0-m Faulkes Telescope North telescope (FTN). A journal of the spectroscopic observations and our instrument configuration is given in Table 3.

All spectra were reduced using the standard IRAF routines, which involves corrections for bias, flat field and cosmic rays. The wavelength calibration is obtained by deriving the dispersion solution using FeAr and FeNe arc lamp spectra. Flux calibration was derived using the instrumental sensitivity curves of spectro-photometric standard stars observed at similar airmass on the same night as the supernova and corresponding standard stars are also listed in Table 3. The spectra were corrected further for continuum atmospheric extinction during flux calibration, using mean extinction curves obtained at Lijiang Observatory in Yunnan and Haleakala Observatory in Hawaii; moreover, telluric lines were removed from the data. The prominent narrow H I emission lines of the host galaxy have also been removed after identifying them using a low-order polynomial to fit the continuum at nearly 6500–6600 Å at the rest-frame wavelength.

3 ANALYSIS

3.1 Reddening

There are two main methods to determine the host-galaxy reddening of SNe Ia: one is the photometric method, based on the correlation found between the light-curve shape and the intrinsic colour (Phillips et al. 1999; Wang et al. 2009; Burns et al. 2014); the other is through the correlation between the equivalent width (EW) of the Na I D absorption feature and the reddening (Munari & Zwitter 1997; Turatto, Benetti & Cappellaro 2003; Poznanski, Prochaska & Bloom 2012). Considering that SNe Iax show large scatter in their observed properties, the photometric method derived from SNe Ia cannot be applied to estimate the host-galaxy reddening for SN 2014ek. On the other hand, the spectra of SN 2014ek do not show obvious Na I D absorption; we thus ignore the host-galaxy extinction and only take into account the Galactic component in the calculation of luminosity. For SN 2014ek, the Galactic reddening is found to be $E(B-V) = 0.054$ (Schlafly & Finkbeiner 2011), corresponding to a *V*-band extinction of 0.17 mag with the Cardelli, Clayton & Mathis (1989) extinction law (i.e. $R_V = 3.1$).

3.2 Light curves

Fig. 2 shows the *UBVRI*- and *gri*-band light curves of SN 2014ek. These light curves cover the phase from about $t\sim-5.2$ days to $t\sim+31.0$ days from the *B*-band maximum light ($B_{\rm max}$). In comparison, the unfiltered observation started four days earlier than the multicolour photometry.

Table 1. Photometric standards in the SN 2014ek field.

	RA	Dec.	U (mag[a])	B (mag)	V (mag)	R (mag)	I (mag)	u (mag)	g (mag)	r (mag)	i (mag)
1	$23^h55^m57.58^s$	$+29^\circ21'43.89''$	16.94(03)	17.04(01)	15.41(01)	14.52(01)	13.63(01)	17.37(01)	16.32(01)	14.73(01)	14.12(01)
2	23:56:16.73	+29:21:52.78	17.66(01)	16.53(03)	15.58(01)	14.53(01)	14.07(01)	16.53(01)	16.78(01)	14.68(01)	14.49(01)
3	23:55:57.53	+29:21:17.25	17.50(01)	17.50(03)	16.89(01)	16.58(01)	16.13(01)	18.33(01)	17.15(01)	16.72(01)	16.55(01)
4	23:56:18.21	+29:21:02.31	18.12(03)	18.24(01)	17.63(01)	17.31(01)	16.85(01)	18.92(02)	17.89(01)	17.46(01)	17.27(01)
5	23:55:53.63	+29:21:19.73	18.90(03)	18.38(01)	17.55(01)	17.15(01)	16.71(01)	19.79(03)	17.95(01)	17.27(01)	17.23(01)
6	23:55:50.63	+29:21:03.1	18.71(03)	18.08(01)	17.15(01)	16.66(01)	16.09(01)	19.59(03)	17.61(01)	16.82(01)	16.54(01)

[a] Note: Uncertainties, in units of 0.01 mag.

Table 2. Optical photometry of SN 2014ek.

MJD	Phase[a] (days)	U (mag)	B (mag)	V (mag)	R (mag)	I (mag)	g (mag)	r (mag)	i (mag)	Unfiltered (mag)	Telescope
56949.00	−9.39	...	...	...	...	...	...	...	...	18.48(44)	TNTS
56952.00	−6.39	...	...	...	...	...	...	...	...	17.88(41)	TNTS
56953.18	−5.21	...	18.17(02)	17.93(04)	17.89(02)	17.46(02)	17.95(03)	17.98(03)	17.74(04)	...	LCO
56953.45	−4.94	...	18.12(04)	17.95(03)	17.82(03)	17.51(04)	17.92(05)	17.91(03)	17.78(06)	...	LCO
56954.04	−4.35	17.44(03)	18.07(01)	17.86(01)	17.68(05)	17.52(03)	...	...	...	...	LJT
56954.99	−3.40	17.55(07)	17.95(01)	17.79(01)	17.59(05)	17.49(03)	...	...	...	...	LJT
56955.99	−2.40	17.46(07)	17.92(01)	17.69(01)	17.50(05)	17.38(03)	...	...	...	...	LJT
56956.00	−2.39	...	...	...	...	...	...	...	...	17.05(64)	TNTS
56958.00	−0.39	...	...	...	...	...	...	...	...	17.33(47)	TNTS
56960.06	1.67	...	17.94(02)	17.55(02)	17.28(04)	17.19(04)	17.70(03)	17.37(05)	17.66(08)	...	LCO
56960.13	1.74	17.68(16)	17.89(02)	17.52(02)	17.34(05)	17.15(03)	...	...	...	...	LJT
56962.14	3.75	...	18.10(03)	17.55(03)	17.32(05)	17.03(05)	17.74(04)	17.51(03)	17.49(04)	...	LCO
56962.17	3.78	17.97(05)	17.81(01)	17.51(01)	17.26(01)	17.02(01)	...	...	...	...	LJT
56962.99	4.60	...	18.08(02)	17.53(02)	17.28(05)	17.10(03)	...	...	...	...	LJT
56965.16	6.77	18.52(05)	18.46(01)	17.61(02)	17.29(05)	17.02(03)	...	...	...	...	LJT
56966.00	7.61	...	18.49(09)	17.59(06)	17.35(05)	17.00(05)	...	...	...	17.40(31)	TNT/TNTS
56967.00	8.61	...	18.53(05)	17.65(03)	17.30(03)	17.01(08)	...	...	...	17.64(30)	TNT/TNTS
56967.08	8.69	...	18.52(06)	17.66(03)	17.34(02)	17.01(01)	...	...	...	...	LJT
56968.00	9.61	...	18.67(08)	17.75(04)	17.36(04)	17.02(05)	...	...	...	17.80(54)	TNTS
56969.12	10.73	...	18.76(06)	17.87(06)	17.40(05)	17.01(09)	18.28(07)	17.65(05)	17.53(05)	...	LCO
56970.00	11.61	...	18.83(05)	17.84(02)	17.39(02)	17.07(02)	...	...	...	17.44(57)	TNT/TNTS
56971.00	12.61	...	18.90(06)	18.04(03)	17.55(02)	17.14(03)	...	...	...	17.60(56)	TNT/TNTS
56971.04	12.65	...	18.83(02)	17.99(01)	17.51(01)	17.07(01)	...	...	...	...	LJT
56972.00	13.61	...	19.16(04)	18.14(02)	17.57(02)	17.19(02)	...	...	...	...	TNT
56973.00	14.61	...	19.41(09)	18.18(02)	17.63(02)	17.25(03)	...	...	...	...	TNT
56973.21	14.82	...	19.35(12)	18.19(08)	17.66(02)	17.22(02)	...	...	...	...	LJT
56976.03	17.64	...	20.03(05)	18.43(02)	17.82(06)	17.38(03)	...	...	...	...	LJT
56977.53	19.14	...	20.32(06)	18.54(02)	17.92(01)	17.31(01)	...	...	...	...	LJT
56980.00	21.61	...	20.37(11)	18.72(04)	18.18(03)	17.61(05)	...	...	...	...	TNT
56981.21	22.82	...	20.45(18)	18.84(06)	18.18(04)	17.63(07)	19.76(09)	18.78(04)	18.44(06)	...	LCO
56982.00	23.61	...	20.44(08)	18.89(03)	18.22(02)	17.71(03)	...	...	...	18.17(38)	TNTS/TNT
56983.17	24.78	...	20.71(10)	18.90(03)	18.30(02)	17.72(02)	...	...	...	...	LJT
56984.00	25.61	...	20.79(11)	18.93(04)	18.32(03)	17.81(06)	...	...	...	18.54(63)	TNTS/TNT
56985.00	26.61	...	20.83(08)	18.96(03)	18.49(03)	17.89(05)	...	...	...	...	TNT
56989.04	30.65	...	20.92(10)	19.14(03)	18.52(02)	17.96(02)	...	...	...	...	LJT
56989.26	30.87	...	...	19.14(08)	18.59(05)	18.05(10)	20.37(09)	19.57(08)	19.19(06)	...	LCO

[a] Relative to the B-band maximum (MJD = 56958.39).

Applying low-order polynomial fits to the light curves near the maximum light yields $m_B(\mathrm{max}) = 17.89 \pm 0.12$ mag on MJD 56958.39 ± 0.34 (2014 October 28.39) and $m_V(\mathrm{max}) = 17.50 \pm 0.04$ mag on MJD 56960.89 ± 0.18 (2014 October 30.39) This corresponds to absolute peak magnitudes of $M_B(\mathrm{max}) = -17.32 \pm 0.23$ mag and $M_V(\mathrm{max}) = -17.66 \pm 0.20$ mag if a distance modulus of 34.99 ± 0.20 mag and a Galactic extinction of $A_V = 0.17$ mag are adopted in the calculation. This indicates that SN 2014ek is apparently fainter than normal SNe Ia but comparable to SN 2002cx and SN 2005hk. Fitting results of the peak apparent magnitude, decline rate within 15 days after the peak and maximum-light date t_{max} in different bands are reported in Table 4. The absolute peak magnitudes, corrected for Galactic extinction, are also presented.

In Fig. 3, we compare the light curves of SN 2014ek with other well-observed SNe Iax, including SN 2002cx (Li et al. 2003), SN 2005hk (Phillips et al. 2007), SN 2011ay (Szalai et al. 2015) and SN 2012Z (Yamanaka et al. 2015). The *BVRI*-band light curves of three

Table 3. Spectroscopic observation of SN 2014ek.

UT Date	MJD	Phase[a] (days)	Exp.(s)	Telescope + Instrument	Range (Å)	Standard Star
2014 Oct. 22	56953.29	−5.10	2400	YNAO 2.4m+YFOSC	3500–9100	Hilt600
2014 Oct. 24	56955.04	−3.35	2400	YNAO 2.4m+YFOSC	3500–9100	BD+28d4211
2014 Oct. 29	56960.17	1.78	2400	YNAO 2.4m+YFOSC	3500–9100	BD+28d4211
2014 Nov. 1	56963.04	4.65	2700	YNAO 2.4m+YFOSC	3600–7400	BD+28d4211
2014 Nov. 3	56965.21	6.82	2400	YNAO 2.4m+YFOSC	3500–9100	Feige15
2014 Nov. 11	56973.21	14.82	2294	YNAO 2.4m+YFOSC	3500–9100	G191B2B
2014 Nov. 15	56977.21	18.82	2700	YNAO 2.4m+YFOSC	3500–9100	Feige110
2014 Nov. 17	56978.68	20.29	3600	FTN 2m+FLOYDS	3200–10 000	Feige34
2014 Nov. 22	56983.68	25.29	3600	FTN 2m+FLOYDS	3200–10 000	Feige34

[a] Relative to the *B*-band maximum (MJD = 56958.39).

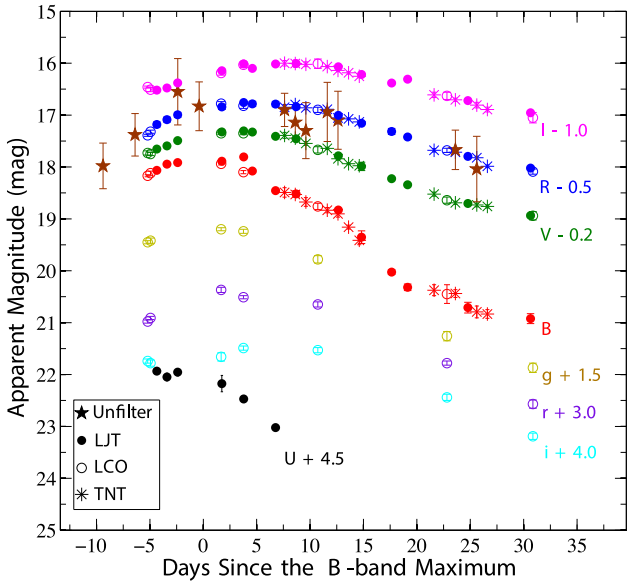

Figure 2. The *UBVRI*- and *gri*-band light curves of SN 2014ek from three different telescopes. Data from LJT 2.4-m, LCO 1-m and TNT 0.8-m telescopes are plotted with solid points, open circles and asterisks, respectively. The unfiltered magnitudes from the TNTS are also overplotted, which are also subtracted by 0.5 mag as the *R*-band data.

representative subclasses of SNe Ia, such as SN 1991T (Lira et al. 1998), SN 1999by (Bonanos et al. 1999), and SN 2005cf (Wang et al. 2009), are overplotted for comparison. The light curves of SN 2007gr (Chen et al. 2014), a typical type Ic supernova, are also overplotted. One can see that the overall light curve evolution of SN 2014ek is similar to that of other comparison SNe Iax (especially SN 2002cx), and it also shows close resemblances to SN 2007gr in the *VRI* bands.

We notice that the *B*-band light curve of SN 2014ek exhibits an abnormal post-maximum evolution, with an apparent break occurring at about 10 days from the maximum light. After $t\sim$+10 days, the *B*-band magnitude shows a faster decline for about one week relative to other comparison SNe, including the subclass of SNe Iax. Such a photometric evolution is also consistent with the rapid flux drop of the continuum on the blue end during this phase (see Section 3.4). This could be explained by a rapid decrease of opacity with the expansion of the ejecta. As such a sudden change in the *B*-band magnitude decline was never seen in other SNe Iax, the fast flux drop might also be due to the newly formed dust in the ejecta.

Unlike normal SNe Ia, SN 2014ek does not show a prominent secondary maximum feature in the *R* or *I* bands, as seen in other SNe Iax. The formation of a secondary peak in the *RI*-band light curve of normal SNe Ia may be related to the opacity or recombination effect (Pinto & Eastman 2000; Kasen 2006). At $t\sim$20–30 days from the peak, the electrons recombine with ions like Fe III and Co II in the ejecta as the photosphere recedes, producing additional emission at this phase, and this leads to the formation of a secondary peak in longer wavebands. For SNe Iax, however, the spectra evolve quickly into the nebular phase because of rapidly decreasing photospheric temperature $T_{\rm eff}$ and photospheric radius $R_{\rm ph}$ soon after the maximum light. As a result, recombination from Fe III to Fe II occurs at a relatively early phase. This may be the reason that SNe Iax show somewhat broader peaks in the *RI* bands. SN 2002cx seems to be an outlier in the *I*-band evolution compared with other SNe Iax, showing a plateau phase of about 20 days (Li et al. 2003), which may result from the mixing of the primary and secondary peaks at a certain level.

In the following analysis, we examine further the explosion time and rise time of the light curve for SN 2014ek. To constrain the pre-maximum-light evolution of the light curves better, the unfiltered data points from the TNTS are also included in the analysis, as shown in Fig. 4. As the unfiltered light curve is very similar to that in the *R* band, we combine them to determine the rise time and explosion date for SN 2014ek. Assuming that the luminosity evolution follows the 'expanding fireball' model (Riess et al. 1999), i.e. $f \propto (t - t_0)^n$ (where f represents the flux and t_0 denotes the first-light time and is also regarded as the explosion time in this article), we derive $t_0 = -14.82 \pm 0.95$ and n= 0.56±0.07 for SN 2014ek (see also the bold solid curve in Fig. 4). This corresponds to a *R*-band rise time of 14.82 ± 0.95 days and an explosion date of MJD 56948.16±0.96. Fitting to the *R*-band light curve of SN 2012Z yields a similar estimate of the rise time, i.e. 14.06±1.69 days. The corresponding rise times of 13.46±0.38 days and 13.14±1.54 days are estimated for SN 2014ck and SN 2011ay, respectively; these are slightly shorter than that of SN 2014ek. In comparison, SN 2005hk seems to show an apparently longer rise time of 16.65±0.25 days. Considering that the explosion time of each band is the same, the deduced rise time to the maximum light of SN 2014ek ranges from ∼10 days in the *B* band to ∼17 days in the *I* band.

3.3 Colour curves

Fig. 5 shows the colour evolution of SN 2014ek and other comparison SNe Iax. The colour curves of different subclasses of SNe Ia are also overplotted. As can be seen, SN 2014ek becomes progressively red after the first detection and it reaches its reddest colour at $t\approx$20–25 days after the maximum light. During the period from $t\sim$ +20 to +25 days, SN 2014ek seems to show the reddest $B - V$ colour among our comparison sample, which is consistent with the

Table 4. Photometric parameters of SN 2014ek.

Parameters[a]	*B*	*V*	*R*	*I*
t_{max} (MJD)	56958.39 ± 0.34	56960.89 ± 0.18	56962.98 ± 0.13	56964.86 ± 0.17
Peak apparent magnitude (mag)	17.89 ± 0.12	17.50 ± 0.04	17.26 ± 0.04	17.02 ± 0.08
Peak absolute magnitude[b] (mag)	−17.32 ± 0.23	−17.66 ± 0.20	−17.86 ± 0.20	−18.06 ± 0.22
Δm_{15} (mag)	1.54 ± 0.17	0.90 ± 0.06	0.71 ± 0.06	0.52 ± 0.11

[a] We take 34.99 ± 0.20 mag as the distance modulus from NED to calculate the absolute magnitude.
[b] Absolute magnitudes have been corrected for the extinction of the Milky Way.

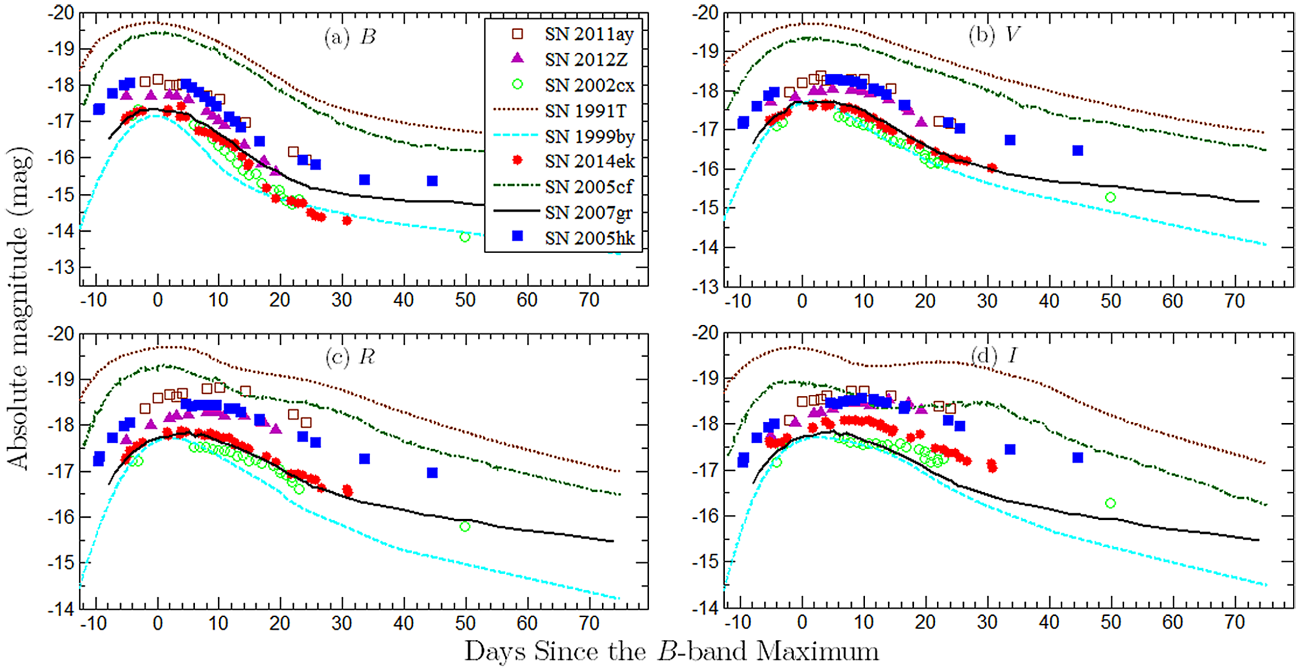

Figure 3. The *BVRI*-band light curves of SN 2014ek, compared with those of other Iax supernovae such as SNe 2002cx (Li et al. 2003), 2005hk (Phillips et al. 2007), 2011ay (Szalai et al. 2015), and 2012Z (Yamanaka et al. 2015). Different subclasses of SN Ia such as SN 1991T (Lira et al. 1998), SN 1999by (Bonanos et al. 1999), SN 2005cf (Wang et al. 2009) are overplotted. The light curves of type Ic supernova 2007gr (Chen et al. 2014) are also plotted for comparison. Note that these light curves have been corrected for the extinctions of the Milkyway and the host galaxies whenever possible.

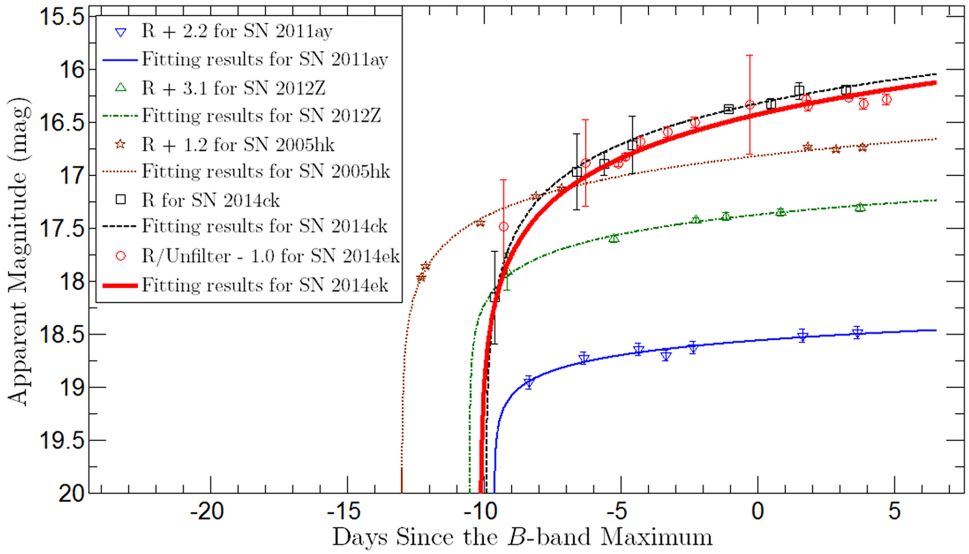

Figure 4. The $f \propto (t - t_0)^n$ model fit to the rise phase of the unfiltered and *R*-band data (open circles). The best-fitting curve is plotted in bold solid line for SN 2014ek. Fits to the rise evolution of some SNe Iax, including SN 2005hk (Phillips et al. 2007), SN 2011ay (Szalai et al. 2015), SN 2012Z (Yamanaka et al. 2015) and SN 2014ck (Tomasella et al. 2016), are also plotted for comparison.

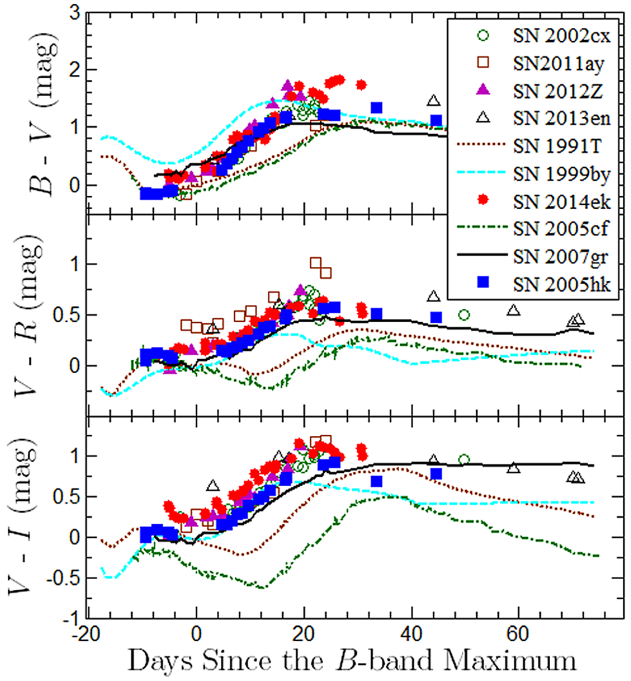

Figure 5. The $B-V$, $V-R$ and $V-I$ colours of SN 2014ek compared with those of SNe 2002cx (Li et al. 2003), 2005hk (Phillips et al. 2007), 2005cf (Wang et al. 2009), 2011ay (Szalai et al. 2015), 2012Z (Yamanaka et al. 2015), 2013en (Liu et al. 2015), 1991T (Lira et al. 1998), 1999by (Bonanos et al. 1999) and 2007gr (Chen et al. 2014). The colour curves have been corrected for Galactic reddening and host-galaxy reddening whenever possible.

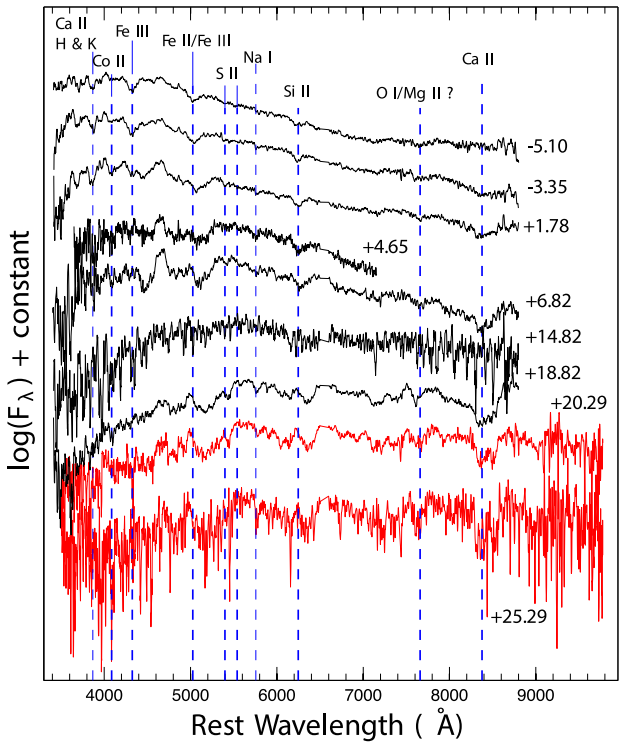

Figure 6. Optical spectral evolution of SN 2014ek. The spectra obtained with the Lijiang 2.4-m telescope are shown in upper region, while those obtained with the LCO FTN 2.0-m telescope are shown in the underside. All of the spectra have been smoothed with a bin of about 14 Å.

deficiency of flux at shorter wavelengths as revealed by spectra at similar phase (see Figure 6). After that, the colour curves evolve bluewards, as similarly seen in other comparison SNe Iax, but large scatter exists in the late-time evolution.

3.4 Spectroscopy

The spectral sequence of SN 2014ek is presented in Fig. 6. These spectra are characteristic of typical SNe Iax, showing weak IMEs and dominant features of Fe II, Fe III and Co II lines. All the spectra have been corrected for the recession velocity of the host galaxy (6933 km s^{-1}). The main lines are labelled in the spectra in light of the identifications obtained in previous studies of SN 2002cx-like object SN 2005hk (i.e. Phillips et al. 2007).

3.4.1 Spectroscopic evolution

To demonstrate the spectral features of SN 2014ek better, we show in Fig. 7 the $t = +1.8$ day spectrum and the synthetic spectrum computed using the SYNAPPS code (Thomas, Nugent & Meza 2011). The SYNAPPS fit gives a black-body temperature of $T_{\rm ph} = 6800$ K and an expansion velocity of $v_{\rm ph} = 5200$ km s^{-1} for the photosphere. The comparison clearly favours the presence of IMEs (Si II, Ca II, S II, C II and O I) and IGEs such as Fe II, Fe III and Co II in the near-maximum-light spectrum. In particular, the prominent Fe II, Fe III and Co II features are reminiscent of the spectral features of the SN 1991T-like subclass, which has much higher photospheric temperature at similar phase, distinguishing SN 2014ek from normal SNe Ia. There are still some minor absorptions that cannot be properly identified for pre-maximum spectra, such as those at ∼6000 and 7000 Å,

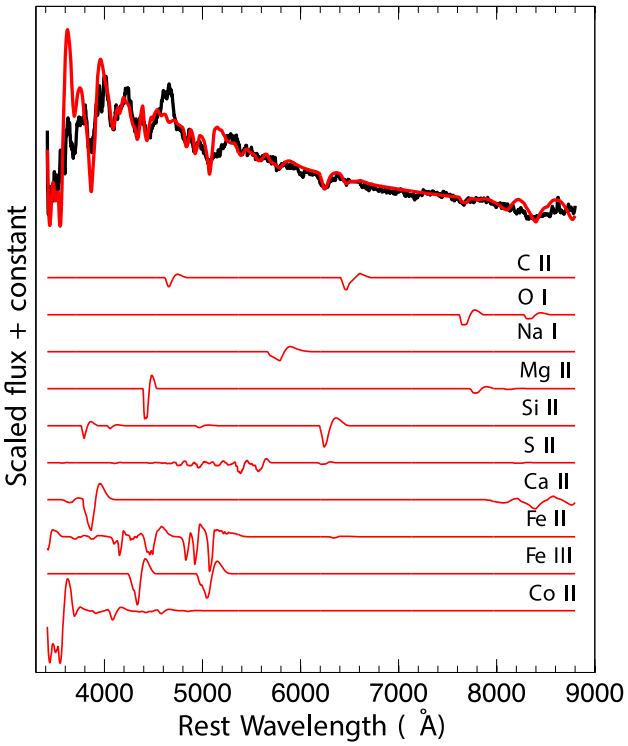

Figure 7. Optical spectrum of SN 2014ek taken at t∼+1.8 days (black). The best-fitting SYNAPPS synthetic spectrum is overplotted. The contribution of each ion is shown in the lower part of the plot.

respectively, though the presence of these features may be affected by the lower signal-to-noise ratio (S/N) of the spectrum. Those minor absorptions are also detected in the pre-maximum spectra of some other SNe Iax such as SN 2011ay and SN 2007qd (McClelland et al. 2010; Szalai et al. 2015); the absorptions at ∼6000 Å can be identified as Fe II, while the absorption at ∼7000 Å might be attributed to O II or C II.

In Fig. 8, we compare the spectra of SN 2014ek with those of some well-observed SNe Iax at $t \sim -5$, +2 and +18 d (relative to the *B*-band maximum), respectively. At t∼5 days before the maximum light, SN 2014ek exhibits a blue continuum and weak absorption of Fe II/Fe III, Si II 6355 and S II lines, similar to SN 2005hk (and perhaps SN 2002cx), while the W-shaped S II and O I 7774 absorption features are clearly detected in SN 2005hk but are almost invisible in SN 2014ek. At this phase, SN 2012Z is found to have relatively broader and stronger line profiles for the above spectral features, in particular the Fe II/III multiplet at ∼5000 Å, perhaps suggesting that it experienced an energetic explosion. At around the maximum light, the Si II 6355, Ca II and Fe II/III lines become stronger in SN 2014ek and the S II and O I lines are visible in the spectrum. The O I λ7774 absorption may be mixed with a very weak Mg II line. In comparison with SN 2014ek, SN 2010ae seems to have relatively deeper and stronger S II and Si II lines at this phase. By t∼2 weeks from the peak, the spectrum is dominated by some features of Fe II lines and the Ca II near-infrared (NIR) triplet. The relative strengths of the three components of Ca II show obvious differences among the comparison SNe Iax. No prominent features of He I lines can be detected in the spectra of SN 2014ek.

3.4.2 *Ejecta velocity*

In this subsection, we examine the ejecta velocity of SN 2014ek inferred from absorption of different ions in the spectra. Fig. 9 shows the velocities inferred from Si II, Ca II, O I and Fe II absorptions. The above velocity measurements may have larger uncertainties due to the lower S/N of the spectra and line blending between different ions. For example, the O I λ7773 line may be mixed with a weak Mg II line according to the SYNAPPS modelling. Assuming one Gaussian component in the fitting of Si II 6355 absorption, we obtained an expansion velocity of ∼5000km s^{-1} for SN 2014ek from the t∼0 day spectrum, which is comparable to other SNe Iax such as SN 2002cx and SN 2005hk at similar phases. For SNe Iax, however, the Si II 6355 absorption tends to blend with the neighbouring Fe II absorption (i.e. Fe II λ6456 Å) soon after the peak and this will make measurements of their Si II velocities biased towards smaller values. For example, the Si II velocity of SN 2011ay was estimated as ∼5600 km s^{-1} near the maximum light by assuming a single feature in the fit (Silverman et al. 2011; Foley et al. 2013), while a much higher Si II velocity (i.e. ∼9000 km s^{-1}) can be determined when considering the contamination of the nearby iron lines (Szalai et al. 2015). For SN 2014ek, the near-maximum-light Si II velocity can increase to ∼7200 km s^{-1} when taking the Fe II contamination into account.

The ejecta velocities derived for SN 2014ek from different ions are overall much lower than the corresponding values of normal SNe Ia and SNe Ibc measured at similar phases. The Si II velocity tends to show a rapid decrease with time, with a gradient of 195 ± 34 km s^{-1} d^{-1}. In contrast, the velocity of the Ca II near-infrared (NIR) triplet remains almost constant during the period from one week before the peak to three weeks after that, which may be because Ca II has a low excitation energy. SN 2012Z shows similar evolution for the velocity of the Ca II NIR triplet (Yamanaka et al. 2015). To make a closer inspection of the velocity evolution among different SNe Iax, we show in Fig. 10 the Si II λ6355 velocity evolution for SN 2014ek and other SNe Iax. It is readily seen that SN 2014ek has a velocity evolution similar to SN 2005hk and SN 2002cx. In contrast, SN 2005cc shows a faster velocity evolution with velocity gradient of 443±70 km s^{-1} d^{-1}, while SN 2008A and SN 2010ae have velocity gradients of 122±52 km s^{-1} d^{-1} and 123±76 km s^{-1} d^{-1}, respectively.

3.5 Bolometric light curve

In this subsection, we construct the bolometric light curve of SN 2014ek using the multicolour light curves presented in Section 3. As this peculiar SN is similar overall to SN 2005hk spectroscopically and photometrically in the optical band, we thus take the *BVRIJHK*-band light curve of the latter as a template to infer the flux contribution in the near-infrared (NIR) bands for the former. For SN 2005hk, the fractional contribution of the NIR flux to the bolometric flux is estimated to vary from 14.5 per cent at $t = -5.2$ days to 28.7 per cent at $t = +31.0$ days, based on the published data from Phillips et al. (2007). This flux ratio of NIR emission is then used to build the pseudo-bolometric light curve of SN 2014ek, as shown in Fig. 11. The bolometric light curves of SN 2005hk and SN 2012Z are overplotted for comparison (Phillips et al. 2007; Yamanaka et al. 2015). A polynomial fit to the light curve of SN 2014ek gives a peak bolometric luminosity of $L_{\rm max} \approx 2.29 \times 10^{42}$ erg s^{-1}, which seems to be fainter than SN 2005hk by a factor of ∼1.3.

With the derived bolometric luminosity, we can estimate the synthesized ^{56}Ni mass. Assuming Arnett's law (Arnett 1982) and that the maximum luminosity can be produced by radioactive ^{56}Ni (Stritzinger & Leibundgut 2005; Ganeshalingam et al. 2012), we estimate the mass of ^{56}Ni produced during explosion as about 0.08 $M_\odot$, consistent with estimates of other SNe Iax, which have a range from 0.03$M_\odot$–0.3 $M_\odot$. Different models have been proposed to explain the observed scatter of the nickel mass synthesized in the explosion of SNe Iax. One of these models is a hybrid C–O–Ne white dwarf with weak pure deflagration (Denissenkov et al. 2015), while the fall-back explosion of massive stars that may be produced by a black hole or a compact star is also proposed (Moriya et al. 2010).

4 DISCUSSION

4.1 Luminosity of SNe Iax

In this subsection, we examined the relations between absolute *VR*-band peak magnitudes and some photometric/spectroscopic parameters including the post-maximum decline rate Δm_{15}, near-maximum-light Si II velocity and peak $V - R$ colour, based on an updated sample of SNe Iax ($N = 45$). The relevant parameters of this SN sample and their host galaxies are listed in Table 5. The ejecta velocity inferred from the Si II absorption line has been proposed to be an important parameter to distinguish different subclasses of SNe Ia (i.e. Wang et al. 2009, 2013). Fig. 12(a) shows the absolute peak *RV*-band magnitudes as a function of Si II velocity measured around the maximum light. Most SNe Iax, including SN 2014ek, seem to have Si II velocities clustering in a narrow range of 4000–5000 km s^{-1}. For SNe Iax within such a velocity range, their luminosity might be correlated with the Si II velocity. Note that there exists a subgroup with lower Si II velocity at around 2000 km s^{-1}, i.e. SN 2008ha, SN 2009J and 2014ck, which show large scatter in their peak luminosity, ranging from −14.0 to −17.5 mag in the *R* band. This complicates our understanding of the

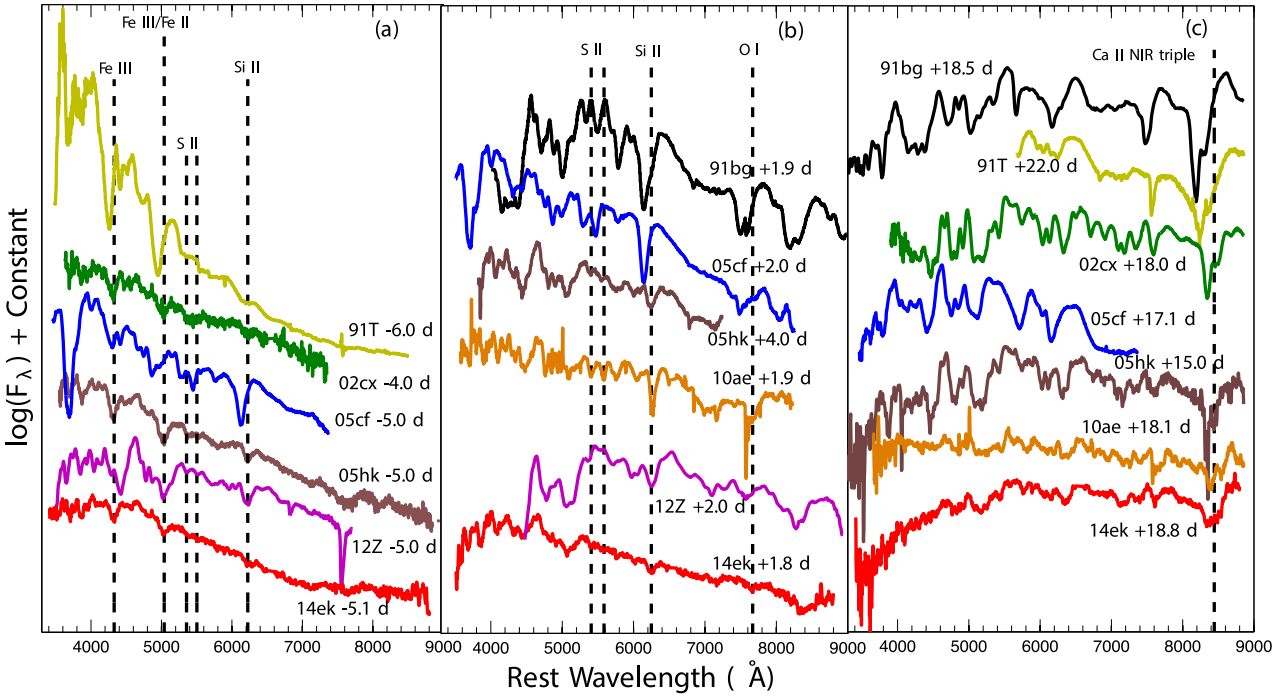

Figure 8. The spectra of SN 2014ek at $t \sim -5.1$, +1.8 and +18.8 days, compared with the spectra of SNe 2002cx (Li et al. 2003), 2005hk (Phillips et al. 2007), 2010ae (Stritzinger et al. 2014), 2012Z (Yamanaka et al. 2015), 2005cf (Wang et al. 2009), 1991T (Mazzali, Danziger & Turatto 1995) and 1991bg (Turatto et al. 1996) taken at similar phases. All spectra shown here have been corrected for the reddening of the Milky Way and redshift of the host galaxy.

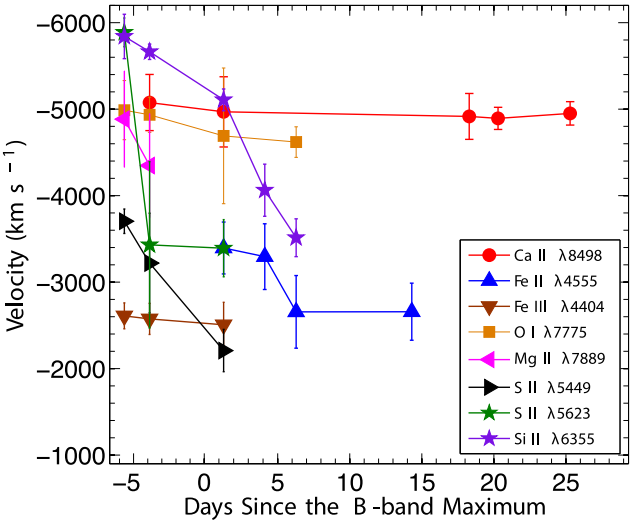

Figure 9. Velocity evolution of some absorption lines in the spectra of SN 2014ek near the *B*-band maximum light.

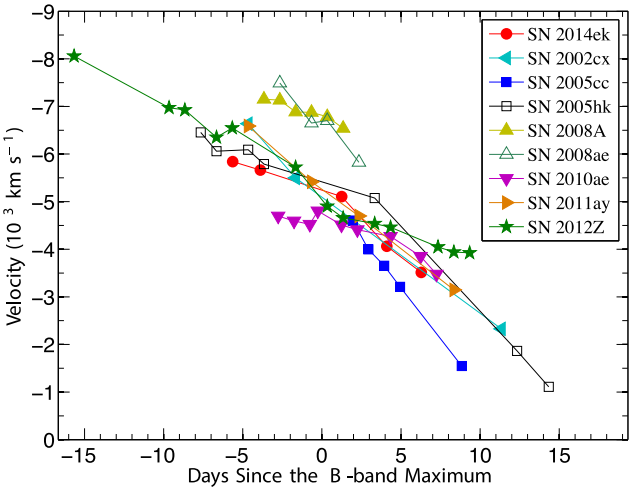

Figure 10. Comparison of velocity evolution of Si II λ6355 between SN 2014ek and some other SNe Iax. Spectra of SN 2005cc are from Blondin et al. (2012), while references for the spectra of other SNe Iax are listed in the last column of Table 5.

luminosity–velocity relation observed for SNe Iax. Fig. 12(b) shows the absolute peak magnitudes $M_{V,R}$(max) plotted against Δm_{15}. SN 2014ek exhibits the properties of a typical SN Iax like SN 2002cx, with a post-maximum decline rate of $\Delta m_{15} = 0.71 \pm 0.06$ mag in *R* and 0.90 ± 0.06 mag in *V*, respectively. An anti-correlation seems to exist between peak magnitude and post-peak decline rate, but it does not hold for the remaining sample when excluding SN 2008ha and SN 2009J, which both have very low luminosity. Thus, a larger sample of SNe Iax with luminosity lying between the luminous and faint ends is needed to confirm or refute this trend. In Fig. 12(c), we show the relation between $M_{V,R}$(max) and the $V_{\rm max} - R_{\rm max}$ colour. One can see that SNe Iax have redder colours than normal SNe Ia on average, but their peak luminosities do not show any significant correlation with the peak $V - R$ colours.

Compared with the subluminous SN 1991bg-like subclass of SNe Ia, SNe Iax have similar peak luminosity but show an obviously slower decline rate and lower ejecta velocity. One possible explanation, proposed by Li et al. (2003), is that a lower ejecta velocity results in a smaller escape possibility and a longer diffusion time-scale for γ-ray photons, which makes the photosphere cool down slowly and gives the SN a slower post-maximum decline rate.

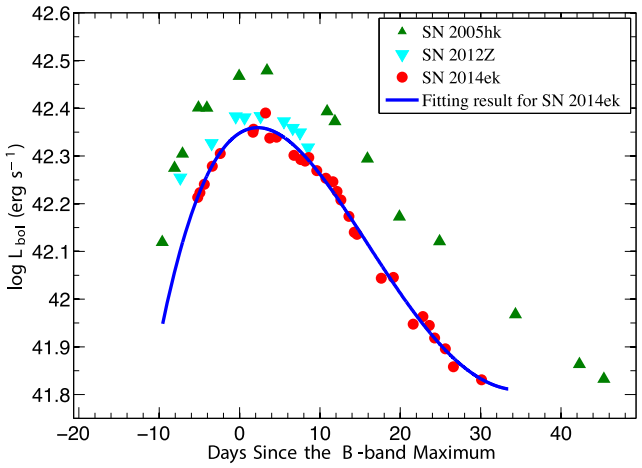

Figure 11. The pseudo-bolometric light curve of SN 2014ek. The polynomial fit to the observed data is shown as a line. For comparison, the pseudo-bolometric light curves of SN 2005hk (Phillips et al. 2007) and SN 2012Z (Yamanaka et al. 2015) are also plotted as triangles and inverted triangles, respectively.

However, the colour evolution of SNe Iax may imply a rapid change of temperature and indicates that there may be some other reasons to explain the low luminosity and slow decline rate of SNe Iax. Nevertheless, the overall lower luminosity suggests a weak explosion for SNe Iax, i.e. with a small amount of ^{56}Ni being produced only at the surface of white dwarfs (Foley et al. 2013).

4.2 Host galaxies

Previous studies have shown that SNe Iax tend to occur in late-type galaxies (i.e. Foley et al. 2009) and SN 2014ek seems to follow this tendency. The host galaxy of SN 2014ek shows a close resemblance to a Sb galaxy based on its morphology from the SDSS images. In order to explore the statistical properties of SN Iax host galaxies, we collect the host-galaxy parameters of 45 SNe Iax from the literature and our own database. These parameters are presented in Table 5, including the host-galaxy morphology, redshift ($z_{\rm Helio}$), radial distribution ($R_{\rm SN}/R_{\rm gal}$), fractional flux in the *ugr* bands (f_u, f_g and f_r) and metallicity of the supernova sites. For the 37 SNe Iax with Hubble types determined or judged for their host galaxies, 29 (with a fraction of 78.3 per cent) are found to occur in Sb-Irr galaxies, seven in Sa-Sba galaxies (SN 2002bp, SN 2006hn, SN 2008A, SN 2011ay, SN 2011ce, SN 2013en and SN 2014cr) and one in an S0 galaxy (SN 2008ge), while none was found in an elliptical galaxy. This indicates that SNe Iax are skewed to the late-type spiral galaxies like core-collapse SNe (i.e. Li et al. 2011), favouring the idea that they should arise from younger progenitor populations. The histogram distributions of host galaxy type for SNe Ia, SNe Iax, SNe Ibc and SNe II are shown in the left panel of Fig. 13. Samples of SNe Ia, SNe Ibc and SNe II in Fig. 13 are taken from Wang et al. (2013). In the right panel of Fig. 13, we further examine the radial distribution of SNe Iax and other subclasses of SNe, which might be related to the age and/or metallicity of the supernova sites. This radial distance from the galactic centre, normalized to the optical radius of the host galaxy, $R_{\rm SN}/R_{\rm gal}$, is available for 31 of our sample of SNe Iax. We found that nearly 43 percent of them are located in regions with $0.4 < R_{\rm SN}/R_{\rm gal} < 0.8$, while this fraction is only about 11 percent for SNe Ibc and 20 percent for SNe II, respectively. This contrast in radial distribution indicates that SNe Iax tend to occur in outer regions of the galaxy and their progenitors may have relatively lower metallicity, but more sample of SNe Iax are needed to confirm this trend.

There are a few measurements of oxygen abundance for the host galaxies of SNe Iax, which are in the range 12+log(O/H)=∼8.16–8.87 (Magee et al. 2017; Lyman et al. 2018), somehow lower than the solar abundance (Caffau et al. 2008). This indicates that the site of SNe Iax may have relatively lower metallicity compared with other subtypes of SNe Ia, but comparable to that of SNe II or SNe Ibc. Note that Lyman et al. (2018) recently carried out an analysis of metallicity for the host galaxies and explosion sites of a large sample of SNe Iax through both integral-field and long-slit spectroscopy and they also found that the SN Iax explosion site metallicity distribution is similar to that of core-collapse SNe.

We also measure the fractional flux of the SN site, which is the fraction for which the total host light in a pixel is fainter than or equal to the light in the pixel at the location of the SN. This parameter can be used to trace the difference/similarity between luminosity at SN locations and the light of the hosts (Fruchter et al. 2006). As the fractional flux is independent of galaxy morphology and size, it is thus a better parameter to quantify the correlation between SN progenitor environments and the light of their hosts (i.e. Wang et al. 2013). Such an analysis can be performed for 21 SNe Iax of our sample by using the host-galaxy images from SDSS DR12 (Alam et al. 2015) and Panstarrs (Chambers et al. 2017); the results are also tabulated in columns (9)–(11) of Table5. The distribution of the fractional fluxes of our SN Iax sample in the *ugr* bands is shown in Fig. 14. The fractional flux distributions of SNe Ia, SNe Ibc and SNe II are overplotted for comparison and the measurements of these samples are taken from Wang et al. (2013). One can see that the progenitor populations of SNe Iax belong to the brighter regions of the host galaxies, similar to the case for SNe Ibc (especially in the *g* and *r* bands), suggesting that SNe Iax may arise in larger star-forming regions that produce more massive stars. This is also evidenced by the Kolmogorov–Smirnov (KS) test results, as tabulated in Table 6. One can see that SNe Iax and SNe Ia trace the host-galaxy light differently, with a very low probability (i.e. $P = 0.04$ in *r*) that they come from the same stellar populations. SNe Iax also show some differences from SNe II in the light distribution of progenitor populations, with KS test results of $P = 0.13$ in *g* and $P = 0.17$ in *r*, respectively. In the *u* band, however, we notice that SNe Iax seem to show large differences from all kinds of SNe in the fractional flux distribution. This is likely related to the relatively larger uncertainty in the SDSS *u*-band photometry. As for the comparison between SNe Iax and SNe Ibc, *P* values of 0.33 obtained in the *g* band and 0.37 in the *r* band indicate that the hypothesis that they share a similar fractional flux (and hence environment) distribution cannot be rejected.

4.3 Progenitors and explosion models

For the 45 objects that are classified as SNe Iax, their ejecta velocities, strengths of absorption lines and peak luminosities show large differences. Most members of the sample are found to be similar to SN 2002cx, such as SN 2014ek presented in this article. There is also a small fraction of SNe Iax showing close resemblance to SN 2008ha. SN 2008ge may belong to another subtype, which shows a very broad light curve relative to SN 2002cx (Foley et al. 2010).

Previous studies indicate that the progenitors of SNe Iax may be a WD with a companion star exploding as weak deflagration (Jordan et al. 2012; Kromer et al. 2013; Fink et al. 2014), consistent with the S II and O I features in their spectra, but this cannot properly explain

Table 5. Host galaxies of SNe Iax samples.

SN	Galaxy	Galaxy Type	$z_{\rm Helio}$	$M_{R,\,\rm peak}$ (mag)	$\Delta m_{15}(R)$ (mag)	$v^0_{\rm Si\,II}$ (10^3 km s^{-1})	$R_{\rm SN}/R_{\rm gal}$ [a]	f_u [b]	f_g	f_r	12+log(O/H)	Reference[c]
SN1991bj	IC 344	Sb	0.018	...	...	...	0.59	...	...	...	8.37(01)	2,3,16
SN1999ax	SCP J140358.12+155106.9	...	0.050	...	...	...	0.56	0.17	0.44	0.44	...	3
SN2002bp	UGC 6332	SBa	0.021	...	...	...	0.93	0.17	0.28	0.38	8.77(25)	3,16
SN2002cx	CGCG 44-035	Sb	0.024	−17.64(15)	0.54(06)	4.71(05)	1.23	0.30	0.60	0.63	8.36(01)	2,3,4,16
SN2003gq	NGC 7407	Sbc	0.021	−17.37(15)	0.71(10)	4.85(12)	0.10	0.75	0.92	0.92	8.33(02)	2,3,16
SN2004cs	UGC 11001	Sc	0.014	...	...	...	0.47	0.88	0.88	0.82	8.43(01)	3,16
SN2004gw	PGC 16812	Sbc	0.017	...	...	...	1.13	...	...	...	...	2,3
SN2005P	NGC 5468	Scd	0.009	...	...	...	0.44	...	...	...	8.36(06)	2,3,16
SN2005cc	NGC 5383	Sb	0.008	−17.13(15)	0.65(01)	4.60(05)	0.05	0.99	1.00	1.00	8.50(02)	2,3,16
SN2005hk	UGC 272	Sd	0.013	−18.07(15)	0.52(13)	4.86(18)	0.45	0.24	0.31	0.26	8.34(09)	2,3,5,16
SN2006hn	UGC 6154	Sa	0.017	...	...	...	0.25	0.85	0.91	0.92	8.50(02)	2,3,16
SN2007J	UGC 1778	Sd	0.017	...	...	...	0.45	...	...	...	8.38(02)	2,3,16
SN2007ie	SDSS J21736.67+003647.6	...	0.093	...	...	...	...	0.00	0.67	0.75	...	17
SN2007qd	SDSS J020932.74-005959.6	Sc	0.043	...	...	2.80(10)	...	0.00	0.16	0.22	8.79(03)	2,3,6
SN2008A	NGC 634	Sa	0.016	−18.41(15)	0.51(01)	5.22(51)	0.38	...	...	...	...	2,3
SN2008ae	IC 577	Sc	0.030	...	...	6.72(07)	0.71	0.47	0.63	0.67	8.50(02)	2,3,16
SN2008ge	NGC 1527	S0	0.004	...	...	...	0.05	...	...	...	...	2,3,7
SN2008ha	UGC 12682	Irr	0.005	−14.28(15)	0.97(02)	2.48(28)	0.31	0.27	0.64	0.69	8.16(15)	2,3
PTF09ego	SDSS J172625.23+625821.4	...	0.104	−18.30	0.25	...	...	...	...	...	...	17,19
PTF09eoi	SDSS J232412.96+124646.6	...	0.042	−16.90	...	...	...	0.15	0.79	0.78	...	19
SN2009J	IC 2160	Sbc	0.016	−15.47(22)	0.79(05)	2.21(10)	0.44	...	...	...	8.41(02)	2,3,16
PTF10xk	...	...	...	−17.30	0.57	...	...	...	...	...	...	19
PTF10ujn[d]	...	...	0.12	...	...	...	...	...	...	...	...	16
SN2010ae	ESO 162-17	Sb	0.004	...	...	4.52(03)	0.20	...	...	...	8.40(18)	3,8
SN2010el	NGC 1566	Sbc	0.005	...	...	...	0.10	...	...	...	8.51(02)	3,9,16
SN2011ay	NGC 2315	Sa	0.021	−18.60(17)	0.82(07)	5.42(04)	0.24	...	...	...	...	3,9
SN2011ce	NGC 6708	Sa	0.009	...	...	...	0.16	...	...	...	...	3
PTF11hyh	SDSS J014550.57+143501.9	...	...	−18.70	0.44	...	...	...	...	...	...	19
SN2012Z	NGC 1309	Sbc	0.007	−17.92(02)	0.52(01)	5.26(18)	0.69	0.11	0.31	0.24	8.51(31)	3,10
PS1-12bwh	CGCG 205-21	Sbc	0.023	...	...	...	0.40	0.71	0.83	0.84	8.87(19)	11,18
iPTF13an	2MASX J12141590+1532096	Sb	0.080	...	...	...	...	0.00	0.31	0.59	...	19
SN2013dh	NGC 5936	Sb	0.013	...	...	...	...	0.96	1.00	1.00	...	20
SN2013en	UGC 11369	Sba	0.015	−18.40(30)	0.55(18)	...	0.55	...	...	...	8.46(03)	12,16
SN2014ck	UGC 12182	Sbc	0.005	−17.29(15)	0.58(05)	2.61(10)	0.13	...	...	...	...	13

Table 5 – *continued*

SN	Galaxy	Galaxy Type	$z_{\rm Helio}$	$M_{R,\,\rm peak}$ (mag)	$\Delta m_{15}(R)$ (mag)	$v^0_{\rm Si\,II}$ (10^3 km s^{-1})	$R_{\rm SN}/R_{\rm gal}$[a]	f_u[b]	f_g	f_r	12+log(O/H)	Reference[c]
SN2014cr	NGC 6806	Sa	0.019	...	...	...	0.30	...	...	...	...	17
SN2014dt	NGC 4303	Sc	0.005	...	...	...	0.31	0.84	0.87	0.92	8.52(02)	16,17
SN2014ek	UGC 12850	Sc	0.023	−17.86(20)	0.71(06)	5.10(03)	0.24	0.93	0.95	0.97	8.50(02)	1,16
SN2014ey	2MASX J15042974+0219591	Sbc	0.031	...	...	...	0.00	...	...	...	8.43(02)	15
SN2015ce	UGC 12156	Sbc	0.017	...	...	...	...	...	...	...	...	17
PS15aic	2MASX J13304792+3806450	Sc	0.056	...	...	...	...	0.00	0.51	0.34	...	17,18
SN2015H[d]	NGC 3464	Sc	0.012	−17.27(07)	0.69(04)	...	0.42	0.71	0.89	0.87	8.50(10)	14,16
OGLE16erd	...	...	0.068	...	...	...	...	...	...	...	...	17
SN2016atw	...	Sbc/Sc	0.065	...	...	...	...	...	...	...	...	17
SN2016ilf	2MASX J02351956+3511426	Sb	0.045	...	...	...	...	...	...	...	...	15,18
SN2017gbb[d]	IC 438	Scd	0.010	$\leqslant$-17.00	...	...	0.52	...	...	...	...	17

[a] The host galaxy radius is taken from the NASA/IPAC Extragalactic Database (NED).
[b] Fractional fluxes in the *u* band, measured with SDSS DR12 and PanSTARRS images.
[c] (1) This article; (2)Foley et al. 2009; (3) Foley et al. 2013; (4) Li et al. 2003; (5) Phillips et al. 2007; (6) McClelland et al. 2010; (7) Foley et al. 2010; (8) Stritzinger et al. 2014; (9) Szalai et al. 2015; (10) Yamanaka et al. 2015; (11) Magee et al. 2017; (12) Liu et al. 2015; (13) Tomasella et al. 2016; (14) Magee et al. 2016; (15) Transient Name Server; (16) Lyman et al. 2017; (17) Guillochon et al. 2017; (18) morphology judged from images on PanSTARRS; (19) White et al. 2015; (20) Jha et al. 2013.
[d] PTF10ujn is classified as a 02es-like supernova in White et al. (2015). The magnitudes for SN 2015H and SN 2017gbb are from the SDSS *r* and *g* bands, respectively.

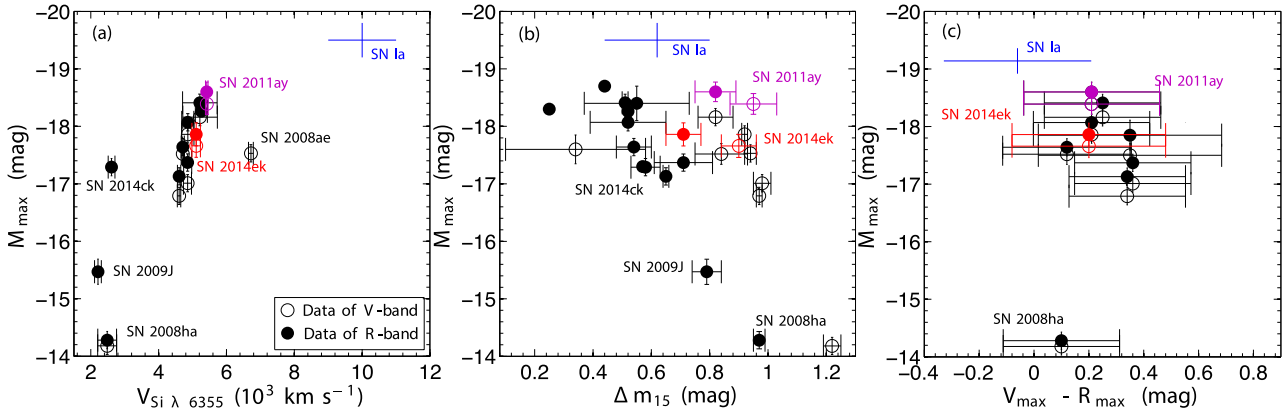

Figure 12. The absolute *VR*-band peak magnitudes plotted against the Si II λ6355 velocity measured around the maximum light, post-peak decline rate Δm_{15} and peak $V-R$ colour for SN 2014ek and other SNe Iax with available photometric and spectroscopic data. The cross represents the ranges of the corresponding parameters obtained for normal SNe Ia.

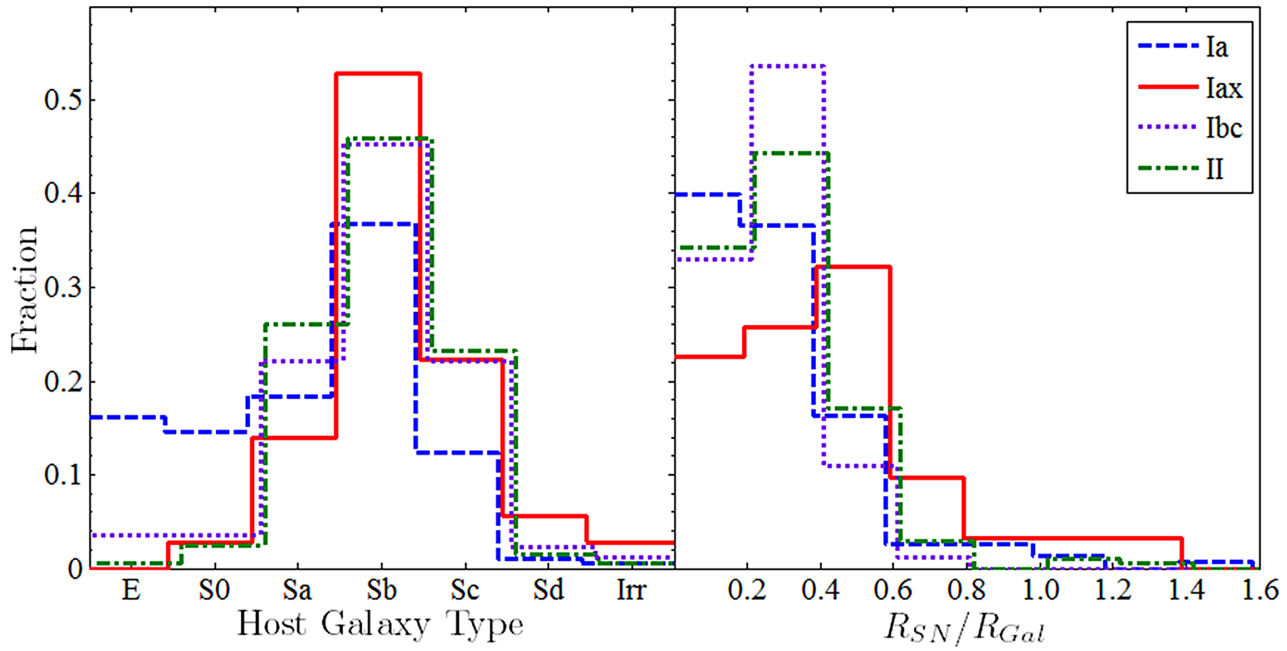

Figure 13 Left panel: Histogram distribution of host galaxy types for SNe Iax, SNe Ia, SNe Ibc and SNe II. Right panel: Histogram distribution of the projected distance of the supernovae from the galactic centre, normalized to the optical radius $R_{SN}/R_{gal,}$ for SNe Iax, SNe Ia, SNe Ibc and SNe II.

the properties of the faint members like SN 2008ha, which was even argued to result from a fallback explosion of massive progenitors (Valenti et al. 2009; Kromer et al. 2015). Moreover, Si II and S II lines are not unique to thermonuclear explosions, which are often seen in the spectra of some SNe Ibc (Valenti et al. 2008; Brown et al. 2007).

On the other hand, analysis of *HST* images prior to the explosion of SN 2012Z shows that its progenitor system is consistent with a blue star, perhaps consisting of a WD and a helium companion (McCully et al. 2014). The pre-explosion *HST* images suggest that the progenitor SN 2008ge should arise from the thermonuclear explosion of a WD star (Foley et al. 2010). However, it should be noted that SN 2008ge may not represent a typical SN Iax, which exploded in a lenticular galaxy with a stellar-population age of 9.5 Gyr. Owing to that, its first spectrum was taken at $t \sim 40$ days after the peak and the exact spectroscopic classification of this object is still uncertain. Moreover, the very broad light curve indicates that it is different from either the SN 2002cx-like SNe Iax or the SN 2008ha-like SNe Iax.

Given the existing subtypes like SN 2002cx, SN 2008ha and perhaps SN 2008ge, it is possible that SNe Iax may have multiple progenitor systems, although the so-called hybrid C–O–Ne WDs progenitor scenario may be able to explain the extremely low ^{56}Ni mass of faint members of SNe Iax (Denissenkov et al. 2015).

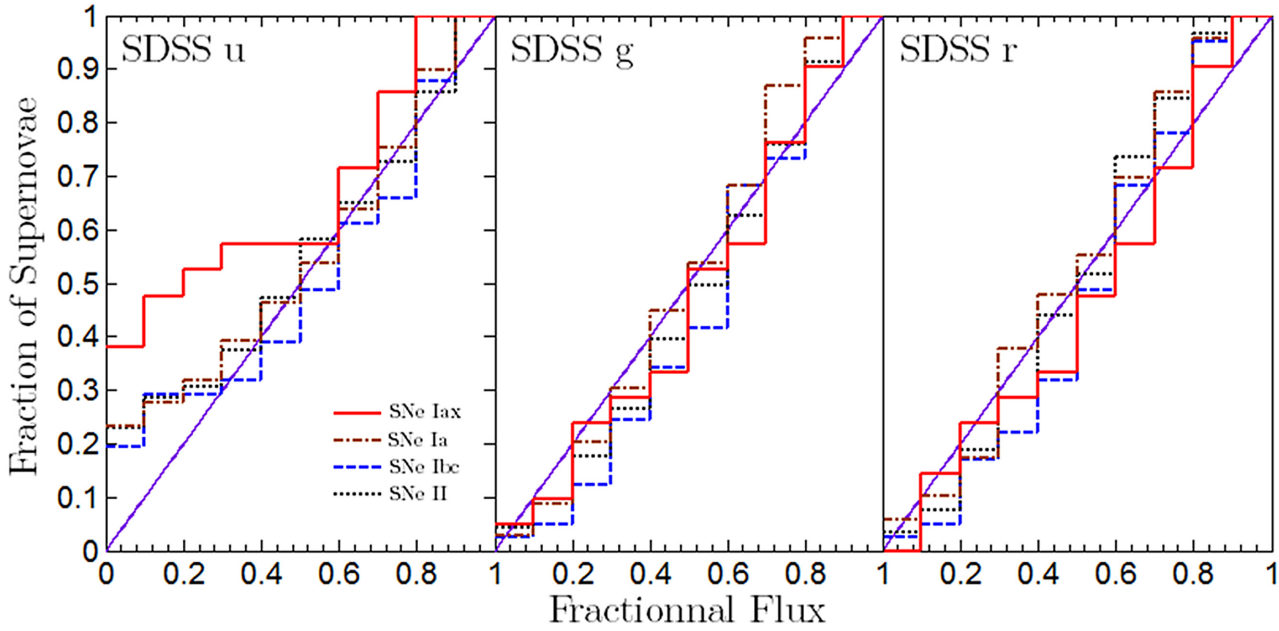

Figure 14. Histogram distribution of the fractional flux of the host-galaxy light at the location of SN progenitors in the SDSS *u*, *g* and *r* bands. The dash–dotted diagonal lines represent the case in which the SN progenitors follow exactly the distribution of the galaxy light.

Table 6. KS test results on the distribution of fractional flux.

SN type	f_u	f_g	f_r
Ia	0.03	0.19	0.04
Ibc	0.05	0.33	0.39
II	0.03	0.13	0.17

5 CONCLUSION

We present the optical photometry and spectra of a 2002cx-like supernova SN 2014ek in this article. SN 2014ek reached its peak magnitude $m_V = 17.50 \pm 0.04$ mag on 2014 October 30.89 UT, with a decline rate of $\Delta m_{15}(V) = 0.90 \pm 0.06$ mag. Combining the early-time light curve with the pre-discovery detection limit, we derive a rise time of ∼14.8 days in the *R* band for SN 2014ek, much faster than a typical SN Ia. At around the maximum light, the Si II velocity is found to be about 5100 km s^{-1} and the absolute magnitude is estimated as -17.66 ± 0.20 mag in *V*, consistent with the values for SN 2002cx and SN 2005hk. Our discovery and follow-up observations of SN 2014ek help further populate the group between overluminous and faint SNe Iax. This peculiar SN also shows similar spectral features and evolution to SN 2002cx and SN 2005hk, but the line strengths in the spectra of SN 2014ek seem to be relatively weaker at late time. We constructed the optical near-infrared pseudo-bolometric light curve of SN 2014ek and found that its peak luminosity was $(\log L)_{\rm max} \approx 42.36$ erg s^{-1}, corresponding to a ^{56}Ni mass of 0.08 $M_\odot$ synthesized in the explosion.

By collecting a large sample of SNe Iax (N= 45) from the literature and our own database, we explored the observed properties of SNe and their host galaxies. We found that the peak luminosity of these SNe Iax might have a loose correlation with their ejecta velocity, decline rate or peak colour, but these weak correlations depend largely on peculiar events like SN 2008ha and SN 2009J in the sample. Furthermore, we found that the hosts of SNe Iax are highly skewed towards late-type spiral galaxies, with more than 78 per cent of the sample coming from Sb or later than Sb-type galaxies and only one in a lenticular galaxy. The distribution of fractional fluxes of the light at SN positions is also explored and SNe Iax tend to be associated with bright, star-forming regions within their host galaxies, which are more similar to those of SNe Ibc rather than SNe Ia and even SNe II. Nevertheless, SNe Iax are found to occur preferentially in relatively outer side of the host galaxy in comparison with other subclasses of SNe (including SNe Ibc), suggesting relatively lower metallicity for their progenitors. These results suggest that SNe Iax, or at least some of them, may arise from young, massive progenitor systems. In the future, it will be interesting to examine whether SN 2008ha-like SNe can be regarded as a members of SN 2002cx-like explosions extending to the faint end or whether they represent stellar explosions with distinct physical mechanisms or progenitor models when a larger sample with similar properties is available.

ACKNOWLEDGEMENTS

We acknowledge the support of the staff of the Lijiang 2.4-m and Xinglong 2.16-m telescopes. Funding for the LJT has been provided by the Chinese Academy of Sciences and the People's Government of Yunnan Province. The LJT is jointly operated and administrated by Yunnan Observatories and Center for Astronomical Mega-Science, CAS. This work is supported by the National Natural Science Foundation of China (NSFC grants 11178003, 11325313 and 11633002) and the National Program on Key Research and Development Project (grant no. 2016YFA0400803). JJZ is supported by the National Science Foundation of China (NSFC, grants 11403096, 11773067), the Youth Innovation Promotion Association of the CAS, the Western Light Youth Project and the Key Research Program of the CAS (Grant NO. KJZD-EW-M06). TMZ is supported by the NSFC (grant 11203034). This work was also partially supported by the Open Project Program of the Key Laboratory of Optical Astronomy, National Astronomical Observatories, Chinese Academy of Sciences. This work makes use of observations from Las Cumbres Observatory. DAH, CM and GH are supported by the

US National Science Foundation grant 1313484. Support for IA was provided by NASA through the Einstein Fellowship Program, grant PF6-170148.

REFERENCES

Ahn C. P. et al., 2012, ApJS, 203, 21
Alam S. et al., 2015, ApJS, 219, 12
Arnett W. D., 1982, ApJ, 253, 785
Blondin S. et al., 2012, AJ, 143, 126
Bonanos A., Garnavich P., Schlegel E., Jha S., Challis P., Kirshner R., Hatano K., Branch D., 1999, Amer. Astron. Soc. Meeting Abstracts, 31, 1424
Brown G. E., Lee C. H., Moreno M. E., 2007, ApJ, 671, L41
Burns C. R. et al., 2014, ApJ, 789, 32
Caffau E., Ludwig H. G., Steffen M., Ayres T. R., Bonifacio P., Cayrel R., Freytag B., Plez B., 2008, A&A, 488, 1031
Cardelli J. A., Clayton G. C., Mathis J. S., 1989, ApJ, 345, 245
Chambers K. C., Pan-STARRS Team, 2017, Amer. Astron. Soc. Meeting Abstracts, 229, 223.03
Chen J. et al., 2014, ApJ, 790, 120
Denissenkov P. A., Truran J. W., Herwig F., Jones S., Paxton B., Nomoto K., Suzuki T., Toki H., 2015, MNRAS, 447, 2696
Filippenko A. V., 1997, ARA&A, 35, 309
Filippenko A. V. et al., 1992, ApJ, 384, L15
Fink M. et al., 2014, MNRAS, 438, 1762
Foley R. J. et al., 2009, AJ, 138, 376
Foley R. J. et al., 2010, AJ, 140, 1321
Foley R. J. et al., 2013, ApJ, 767, 57
Fruchter A. S. et al., 2006, Nature, 441, 463
Ganeshalingam M. et al., 2012, ApJ, 751, 142
Guillochon J., Parrent J., Kelley L. Z., Margutti R., 2017, ApJ, 835, 64
Howell D. A. et al., 2006, Nature, 443, 308
Huang F., Li J.-Z., Wang X.-F., Shang R.-C., Zhang T.-M., Hu J.-Y., Qiu Y.-L., Jiang X.-J., 2012, RAA., 12, 1585
Jha S., Branch D., Chornock R., Foley R. J., Li W., Swift B. J., Casebeer D., Filippenko A. V., 2006, AJ, 132, 189
Jha S. W. et al., 2013, The Astronomer's Telegram, 5143
Jordan G. C.,, IV, Perets H. B., Fisher R. T., van Rossum D. R., 2012, ApJ, 761, L23
Jordi K., Grebel E. K., Ammon K., 2006, A&A, 460, 339
Kasen D., 2006, ApJ, 649, 939
Kromer M. et al., 2013, MNRAS, 429, 2287
Kromer M. et al., 2015, MNRAS, 450, 3045
Lira P. et al., 1998, AJ, 115, 234
Liu Z.-W. et al., 2015, MNRAS, 452, 838
Li W. et al., 2003, PASP, 115, 453
Li W. et al., 2011, MNRAS, 412, 1441
Lyman J. D., James P. A., Perets H. B., Anderson J. P., Gal-Yam A., Mazzali P., Percival S. M., 2013, MNRAS, 434, 527
Lyman J. D. et al., 2018, MNRAS, 473, 1359
Magee M. R. et al., 2016, A&A, 589, 89
Magee M. R. et al., 2017, A&A, 601, 62
Mazzali P. A., Danziger I. J., Turatto M., 1995, A&A, 297, 509
McClelland C. M. et al., 2010, ApJ, 720, 704
McCully C. et al., 2014, Nature, 512, 54
Moriya T., Tominaga N., Tanaka M., Nomoto K., Sauer D. N., Mazzali P. A., Maeda K., Suzuki T., 2010, ApJ, 719, 1445
Munari U., Zwitter T., 1997, A&A, 318, 269
Perlmutter S. et al., 1999, ApJ, 517, 565
Phillips M. M., 1993, ApJ, 413, L105
Phillips M. M., Lira P., Suntzeff N. B., Schommer R. A., Hamuy M., Maza J., 1999, AJ, 118, 1766
Phillips M. M. et al., 2007, PASP, 119, 360
Pinto P. A., Eastman R. G., 2000, ApJ, 530, 757
Poznanski D., Prochaska J. X., Bloom J. S., 2012, MNRAS, 426, 1465
Riess A. G. et al., 1998, AJ, 116, 1009
Riess A. G. et al., 1999, AJ, 118, 2675
Scalzo R. A., Aldering G., Antilogus P., 2010, ApJ, 717, 1073
Schlafly E. F., Finkbeiner D. P., 2011, ApJ, 737, 103
Silverman J. M., Filippenko A. V., Barth A. J., Walsh J. L., Assef R. J., 2011, Central Bureau Electronic Telegrams, 2681
Stritzinger M., et al., 2002, AJ, 124, 2100
Stritzinger M., Leibundgut B., 2005, A&A, 431, 423
Stritzinger M. D. et al., 2014, A&A, 561, 146
Szalai T. et al., 2015, MNRAS, 453, 2103
Thomas R. C., Nugent P. E., Meza J. C., 2011, PASP, 123, 237
Tomasella L. et al., 2016, MNRAS, 459, 1018
Tully R. B. et al., 2013, AJ, 146, 86
Turatto M., Benetti S., Cappellaro E., 2003, From Twilight to Highlight: The Physics of Supernovae, ESO ASTROPHYSICS SYMPOSIA (European Southern Observatory), Springer, Berlin, Heidelberg, p. 200
Turatto M., Benetti S., Cappellaro E., Danziger I. J., Della Valle M., Gouiffes C., Mazzalli P. A., Patat F., 1996, MNRAS, 283, 1
Valenti S. et al., 2008, ApJ, 673, L155
Valenti S. et al., 2009, Nature, 459, 674
Valenti S. et al., 2016, MNRAS, 459, 3939
Wang X., Wang L., Filippenko A. V., Zhang T., Zhao X., 2013, Science, 340, 170
Wang X. et al., 2009, ApJ, 697, 380
White C. J. et al., 2015, ApJ, 799, 52
Yamanaka M. et al., 2009, ApJ, 707, L118
Yamanaka M. et al., 2015, ApJ, 806, 191
Yao X., et al., 2015, AJ, 150, 107
Zhang J., Wang X., 2014, The Astronomer's Telegram, 6611
Zhang J.-J., Wang X.-F., Bai J.-M., Zhang T.-M., Wang B., Liu Z.-W., Zhao X.-L., Chen J.-C., 2014, AJ, 148, 1
Zhang T.-M. et al., 2015, RAA., 15, 215

This paper has been typeset from a TEX/LATEX file prepared by the author.